Society of Petroleum Engineers

SPE-189296-STU

Pore-Scale Experimental Study of Matrix-Fracture Interactions during Tertiary Gas Injection in Carbonates Using X-Ray Microtomography

Mohammad Sabti, University of Wyoming

This paper was prepared for presentation at the SPE International Student Paper Contest at the SPE Annual Technical Conference and Exhibition held in San Antonio, Texas, USA, 9-11 October 2017.

Abstract

Fractured oil reservoirs, which are among the most technically complicated oil and gas reservoirs, often trap significant amounts of recoverable oil within the matrix. Extraction of this oil requires a better insight of the main displacement physics controlling matrix-fracture interactions. Immiscible gas injection, for example, is one of the common techniques used to improve oil recovery from fractured reservoirs. However, the presence of fractures in such reserves as a high permeable path impacts the displacement physics and consequently the oil recovery, especially where three phases (*i.e.*, brine, oil, and gas) coexist.

In this study, I performed a set of two- and three-phase experiments under tertiary gas injection using spreading oil on a fractured 10-mm diameter limestone rock sample by utilizing micro-CT imaging technique. The aim is to compare pore fluid occupancies under a wide range of oil saturations within the pore space and the fracture openings. Interpretation of the micro-scale images helps to capture a detailed map of the fluid arrangements within the pore space in the matrix and the fracture. These maps clearly demonstrated the relevance of spreading phenomena to fluid displacements in the fracture undergoing three-phase flow processes.

The saturation profile over the course of the gas injections showed that brine was predominately produced first since it was the most well-connected phase. After increasing the gas flow rate, the gas obtained sufficient capillary pressure to invade areas containing trapped oil at which point oil layers began to form and re-connect the oil phase. The oil layers allowed the further production of oil with each incremental increase in gas flow rate. Oil layers were seen to be thicker at lower flow rates and became progressively thinner with increased capillary number. Overall, it was found that, at higher oil saturations, the displacement of oil was predominantly achieved by the connectivity of the bulk oil after the evolution of the reconnected trapped oil blobs in the matrix, whereas at lower oil saturations, the displacement of oil was governed by the stability and the hydraulic connectivity of the spreading oil layers that maintained the continuity of the oil phase from the matrix to the fracture.

Introduction

Most carbonate reservoirs,which comprise more than half of the world's oil reserves, are naturally fractured with low matrix porosity (Islam 2014). In these formations, the high capillarity contrast between the matrix block and the fracture conduit may lead to poor oil recovery that can typically only reach to less than 30% (Lu *et al*. 2015). This low oil recovery is often due to the early breakthrough of the injected fluid travelingthrough the highly permeable fracture. Despite the remarkable resultson oil recovery from fractured systemsin theliterature (Alajmi 2000; Alvarado*et al*. 2006; Haugen*et al*. 2010), the physics of the displacement mechanisms responsible for the matrix-fracture interactions,which significantly contribute tothe oil recovery are still poorly understood. Thiscould be due to the complexities of the fractures morphology or the limitations of the available experimental resources and technology.

However in such complex systems and when designing an enhanced oil recovery (EOR) project, it is of paramount significance for a reservoir simulation engineer to considerthe matrix-fracture interactions and explore what mechanisms of flow are responsible for displacing the fluids from the matrix to the fracture, especially under three-phase flow.Better understanding of these flow behaviors will certainly help to improve the simulation inputs. For example, running a reservoir simulation to predict oil recovery from fractured reservoirs requires to use macroscopic multiphase flow properties such as capillary pressures and relative permeability as direct inputs. These propertiesmay nevertheless become erratic fordual-porosity and dual-permeability systemsat low oil saturations when different flow mechanisms play a role. One of the pore-scale flow mechanisms concepts manifested during three-phase flow is the spreading phenomena. It can occur when a drop of oil is placedon a surface ofwater in the presence of air. The ability of oil to spread on the surface of water can be described by the spreading coefficient C_{so} as shown in the equation below (Adamson and Gast 1967; Hirasaki 1993; Rowlinson and Widom 2013):

$$C_{so} = \sigma_{gw} - \sigma_{go} - \sigma_{ow}$$

where σ_{gw}, σ_{go}, and σ_{ow} are the interfacial tensions (IFTs) of gas-water, gas-oil, and oil-water pairs of fluids, respectively. When three-phase (brine, oil, and gas) coexist in a system that is under equilibrium, the equilibrium spreading coefficient can either be zero or negative. Depending on the interfacial tensions (IFTs) between each pair of fluids, a zero (or slightly negative) valuemeans that oil will spontaneously spread as a layer between water and gas whereas a negative value means that oil will form a small floating lens on the surface of water in the presence of gas (Blunt 2017). It is assumed based on Neumann's triangle balance (Rowlinson and Widom 2013; Blunt 2017) that $\sigma_{gw} > \sigma_{go} > \sigma_{ow}$. This means that for a spreading system, the equilibrium spreading coefficient cannot be positive. One of the processes during which the spreading phenomena can occur is gas injection into carbonate reservoirs. It is one of the most common EOR schemes in carbonates (Manrique *et al*. 2007; Islam 2014), where three-phase flow of water, oil, and gas can be encountered.During gas injection,oil more likely can spread on the surface of water forming thin layers that occupy the roughness of the fracture wallsand crevices of the pore space, effectively barricading the gas to contact water (Blunt *et al*. 1995, Piri and Blunt 2004). Draining of oil through these spreading layers when they are stable and connected is known as *layer drainage*. This process isslow, but it can ultimately lead to low oil saturations over time (Blunt 2017).

A substantial body of work in literature have been devoted to better understand the impact of the spreading characteristics on residual oil saturation under three-phase flow for nonfractured systems (Chatzis *et al*. 1988; Vizika 1993; Ørenand Pinczewski 1994; Blunt *et al*. 1995; Kalaydjian *et al*. 1995; Dong 1995; Keller *et al*. 1997; Feali *et al*. 2012). Most of these research initiatives have been dedicated to investigating how fluids move through the pore space and what mechanisms of flow are responsible for oil displacement in the presence of spreading oil layers. Blunt *et al*.(1995) investigated the importance of these layers theoretically and experimentally with an extensive discussion on the fundamental mechanisms of oil recovery through these layers in a water-wet porous media. The authors indicated that draining of oil through these layers

depends on their thickness and stability, the flow rate of oil, and the fluids distribution. They performed gravity drainage experiments using sand columns and capillary tubes and concluded that the stability of oil layers in the spreading system provided a continuity of the oil phase. This provided higher oil recovery for the spreading system and in contrary less for the nonspreading system. Since the work of Dumore and Schols in 1974, it has been acknowledged that the residual oil saturation can be as low as few percent due to the gravity drainage through the oil films in the presence of gas and water (Dumoreand Schols 1974; Blunt*et al*. 1995). Zhou and Blunt (1997) obtained a remaining oil saturation as low as 0.1% in their sand pack experiments. The results from a glass micro-model experiment by Øren and Pinczewski (1995) were also consistent with Zhou and Blunt (1997) results as they clearly showed the three-phase fluids distribution where the oilwas distributed in a thin layer between water and gas phases under positive initial spreading coefficient. A Recent study by Feali *et al*. (2012) confirmed the above results using a high-resolution microtomography technique. They directly visualized the distribution of water, oil, and gas at the pore-scale under different spreading conditions on a Bentheimer sandstone sample.

During the last several years, researchers and scientists have been strongly attracted to the use of the micro-CT imaging technique, which has been evolving day-by-day with superior imaging capabilities and resolutions than can reach up to the few hundred nanometer scale. This powerful techniquehas proved overtime that it can certainly be utilized to characterize complex porous geometry and topology such as fractures. Direct visualization of the arrangement of fluids and their movement through the pore space provides better insights into the fundamentals of multi-phase flow in porous media (Andrä *et al*. 2013; Wildenschild and Sheppard 2013).

The main goal of this study was to investigate how the matrix block interacted with the fracture conduit when oil spreadability played a role. A high-resolution micro-tomography imaging technique was utilized to achieve this goal by mapping the pore fluid occupancies in the matrix and the fracture during the three-phase brine, oil, and gas flow processes.

Materials and experimental methodology

In this section, detailed information about the fractured rock sample as well as the fluid properties is given. Then, the experimental setup and procedures used to perform the three-phase flow tests in this work are discussed.

Rock Properties

The flow tests were performed on a 10-mm diameter and 48-mm long miniature fractured limestone core sample called "*Fond Du Lac*".It is a water-wet dolomitic limestone, quarried from an outcrop area in Wisconsin, USA,consisting primarily of calcium carbonate. The fractured core sample was prepared by the following steps: (1) a core plug (38 mm in diameter and 120 mm in length) was cut from a block of Fond Du Lac limestone using water as a cooling medium, (2) the core plug was dried in an oven at 110 °C for 24 hours, (3)porosity and absolute permeability of the core plug were measured, (4) a fracture was introduced into only half of the core plug, (5) the fractured core plug was scanned using medical CT scanner, with a resolution of 256 microns, to visualize the fracture and its orientation throughout the core plug, and (6) two miniature fractured core samples (10 mm in diameter and 48 mm in length) were drilled from the core plug using air as a cooling medium. One of which was usedin the experiment and the other was kept as a backup sample. Both the core plug and the final fractured core sample are shownin Figure 1(a). Table 1 lists all the petrophysical and geometrical properties of the miniature core sample. The fracture was induced by applying a non-uniform stress parallel to the stress axis of the core plug using the modified Brazilian test (Guo *et al*. 1993; Alajmi and Grader 2000; Alajmi 2003). The direction of the stress controlled the topological orientation of the fracture; whether it wasalong the bedding plane or perpendicular to it. Figure 1(b) shows the fracture orientation as it was only extended to the middle of the sample. This was to study

the pore fluid occupancies and the displacement physics at different locations of the specimen including the matrix-only, the fracture, and the matrix surrounding the fracture sites in the sample.

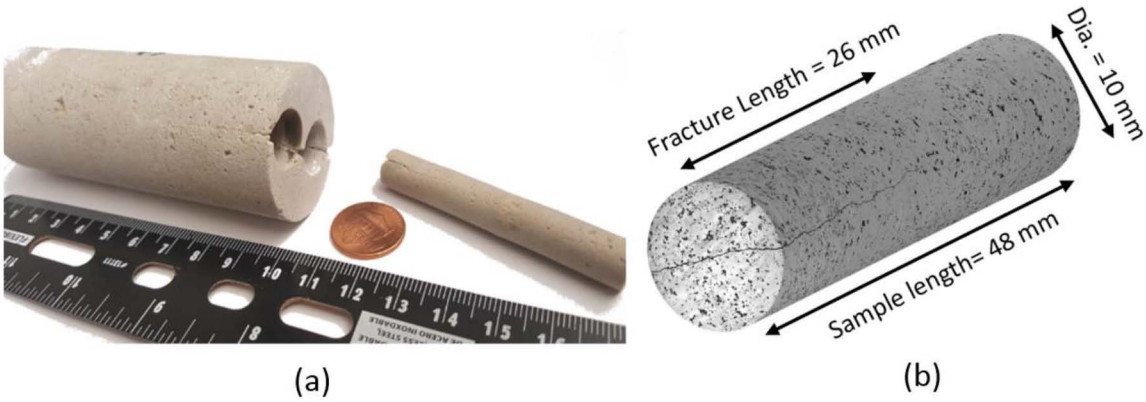

Figure 1—(a) The core plug and the drilled miniature core sample, and (b) a three-dimensional representation of the core sample.

Table 1—Dimensions and petrophysical properties of the miniature core sample used in the experiments.

Rock	Length(mm)	Diameter(mm)	Porosity of the matrix(%)*	Gas Permeability of the matrix(mD)*	Pore volume(ml)
Fond Du Lac limestone	47.98	9.98	10.9	13.8	0.4

*Porosity and absolute permeability (Klinkenberg corrected) were measured on the core plug before creating the fracture using an automated helium porosimeter-permeameter.

Fluid Properties

The aqueous phase (*i.e.,* the wetting phase) was prepared using distilled water, 2 wt% $CaCl_2$, 15 wt% NaI (an X-ray doping agent), and 0.01 wt% NaN_3 (an anti-bacterial growth agent). To avoid dissolution of the limestone matrix during the flow tests, a sacrificial limestone core was immersed in the aqueous solution to be equilibrated with the rock for 24 hours. The oil phase (*i.e.,* the intermediate-wetting phase) was Soltrol 170, which was well purified before use using a gravity glass column filled with alumina and silica gel to remove polar componentswhich may alter the wettability of the rock. The oil phase was also X-ray doped using 5 vol% 1-iodooctane ($C_8H_{17}I$). The gaseous phase (*i.e.,* the most non-wetting phase) was nitrogen with 99.9% purity.The concentrations of the doping agents NaI and 1-iodooctane were determined prior tostarting the experiment to ensure sufficient contrasts between brine, oil, gas, and grains. The fluid system used in this work wasdesigned to be under spreading condition. The spreadability of oil was already tested in previous studies (Sabti*et al*. 2014a;Sabti*et al*. 2014b; Alizadeh and Piri (2014a) and in a micromodel experiment as well using the same fluids used in this study. Soltrol 170 and brine, nitrogen and Soltrol, and nitrogen and brine IFT values reported by Alizadeh and Piri (2014a) for a fluid system using the same brine, oil, and gas used in this work under 800 psig and ambient temperature were 40.77, 20.96, 61.71 mN/m, respectively. These IFT values resulted in an equilibrium spreading coefficient C_{so} of -0.02 which represents a spreading system as explained earlier. Table 2 lists the properties of the fluids used in the present study.

Table 2—Properties of the fluids used in this study.

Fluid	Viscosity(mPa.s)	Density(kg/m³)
Doped brine (2 wt% $CaCl_2$+15 wt% NaI+0.01 wt% NaN_3)	1.145	1138.12
Soltrol 170 (5 vol% 1-iodooctane)	2.526	802.13
Gas (Nitrogen)	0.0187	62.84

Experimental Setup

The state-of-the-art laboratory setup used in this work was designed to carry out two- and three-phase flow experiments at the pore-scale. It consisted of a three-phase miniature core-flooding system integrated with a high-resolution micro-CT scanner. The imaging system was Xradia 510 Versa micro-CT scanner manufactured by Zeiss. It had a wide range of geometric magnifications with different objectives and various source filters. This imaging device could acquire a true spatial resolution up to 700 nm depending on diameter, length, type, and structure of the specimen.The in-house custom-designed core holder, vertically mounted inside the scanner champer, was fabricated from carbon fiber because it is fully X-ray transparent and lightweight as well as having a high strength-to-weight ratio. The core-holder was constructed to allow most lines, from the core-flooding setup, connected to it to be housed inside the micro-CT scanner enclosure. The core-flooding system composed of an array of Rosemount differential pressure transducers with different scales, a three-phase separator, two accumulators, six dual-cylinder 5000 series Quizix® pumps, and a vacuum pump. As shown in Figure 2, three out of the six pumps were utilized to inject the brine, oil, and gas, respectively. An overburden pressure pump was used to maintain a fixed net confining pressure around the core. The other two pumps were used to regulate the pore pressure and compensate for the fluctuations in separator pressure. The design of the core-flooding setup allowed for the equilibration of the three fluids (water/oil/gas) in a closed-loop bypassing the core prior to starting the experiment to avoid any mass transfer between the phasesduring the experiment.

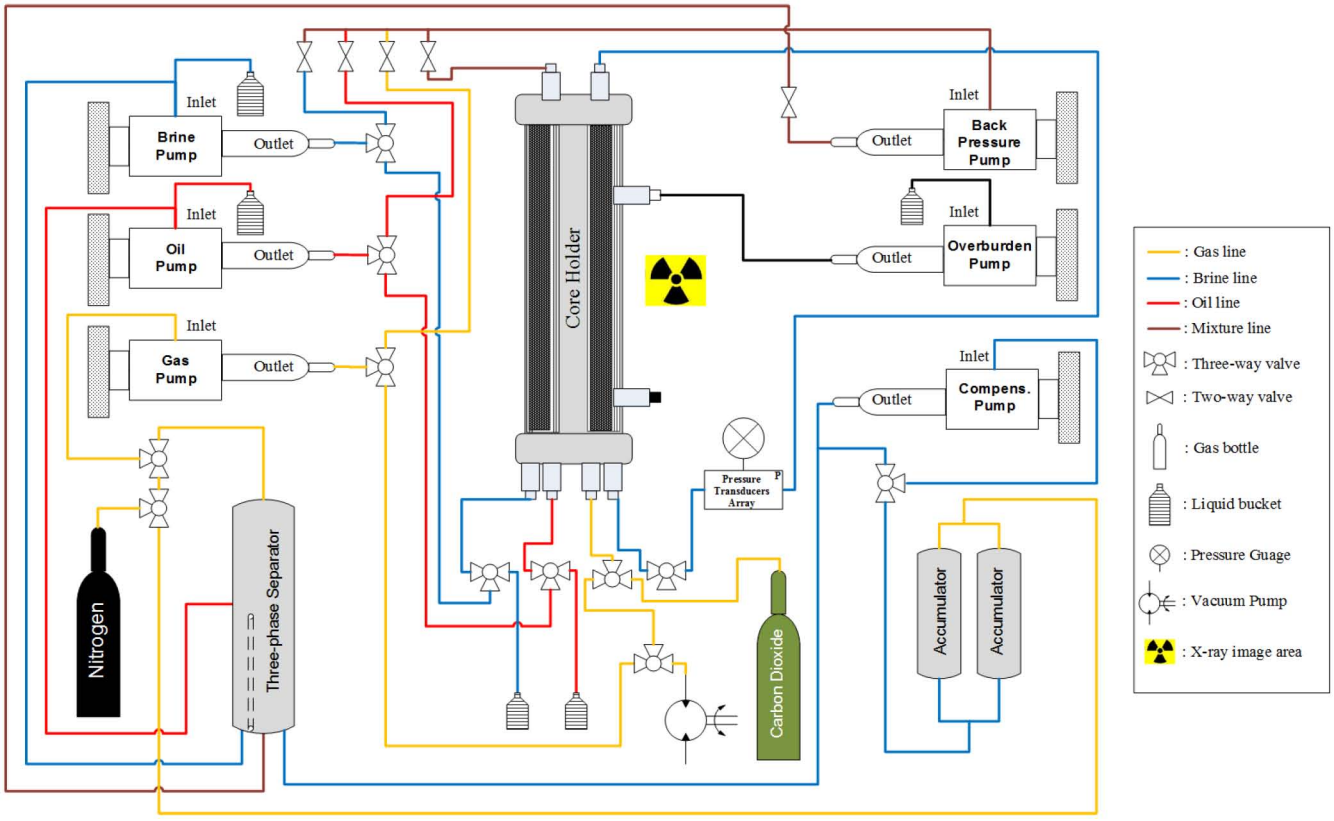

Figure 2—The three-phase core-flooding setup used to perform the experiment. The core holder was placed inside the micro-CT scanner's enclosure (Piri 2012).

Experimental Procedure

A schematic illustration of the experimental procedure used in this work is shown in Figure 3. The experiment was carried out at a pore pressure and temperature of 500 psig and 20°C, respectively. During each step of the experiment, only one fluid was injected into the core (*i.e.*, an unsteady-state approach).

All fluids were injected into the bottom of core sample (the fracture end). The confining pressure was 600 psig(net overburden pressure of 100 psi) and was kept constant during all the injection steps. After mounting the core holder inside the CT scanner chamber, the core was flooded with dry gaseous carbon dioxide CO_2 to remove air and then vacuumed for 24 hours. Subsequently, a dry scan image for the entire length of the sample was acquired under theambient condition to be used as a preliminary scan image of the pore space and the fracture aperture. Afterward, the core sample was vacuum saturated with degassed doped brine (see Table 2) to establish fully brine saturated core (S_w=1). This brine had to be replaced by a low salinity brine (*i.e.,*2 wt% $CaCl_2$ and 0.01 wt% NaN_3) under the experimental conditions to generate an accurate pore space map. The main reason for replacing the doped brine was because it would be difficult to segment the doped brine from the grains to get the reference scan.Doped brine contained 15% NaI (X-ray doping or contrast agent), which was enough to providesimilar contrasts between the doped brine and the grains in the images. After completely displacing the doped brine with the low salinity brine, a wet reference high-resolution scan was obtained. This wet reference scan was obtained under the experimental conditions and used to map the fracture, obtain the porosity distribution as seen in Figure 4, and later measure fluid saturations in the course of the experiments. Table 3 shows the microtomography parameters used to scan the core sample during the flow tests. The core sample was then subjected to an oilflood with an initial flow rate of 0.0001 ml/min followed by a gradual increase to 0.004 ml/min. This was done to establish an average water saturation of 24%. During oil drainage, the pressure drop across the core sample was recorded, and quick scans were performed every ten hoursata low resolution to monitor water and oil saturations. After establishing the desired two-phase initial condition, water was flooded into the core at an initial flow rate of 0.0001 ml/min with a ramping increase to 0.004 ml/min that corresponded to a capillary number of around 10^{-6}. To ensure the residual oil saturation was reached and no further oil would be displaced, the brine flow rate was increased to 0.006 ml/min and the oil saturation was calculated and compared to the previous flow rate. This resulted in a residual oil saturation of 52%. Gas was then injected into the core sampleat various flow rates to reach different oil saturations. During gas injection (*i.e.*, tertiary gas injection (TGI)), the fluid saturations were measured in both the fracture and the matrix.High-resolution scans of 2.5 μm were acquired at the end of each step mentioned above when the saturations no longer changed.

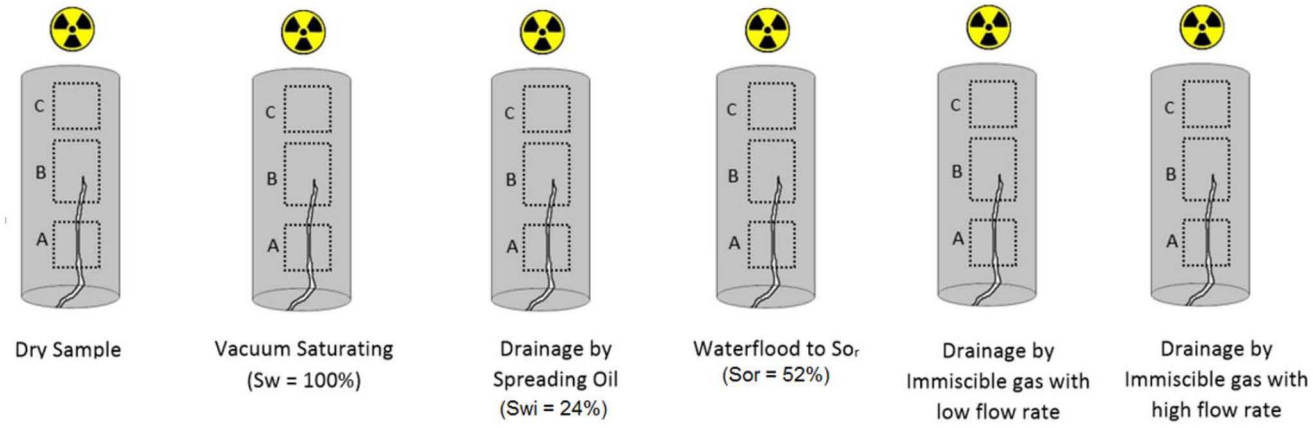

Figure 3—Schematic illustration of the experimental procedure used in this work.

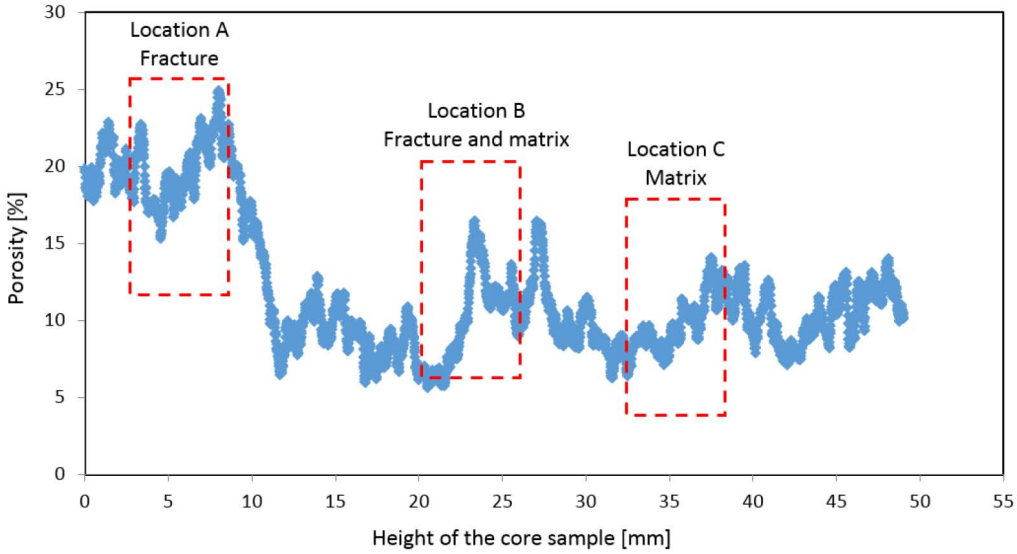

Figure 4—Porosity distribution along the fractured core sample.

Table 3—Microtomography parameters used to scan the core sample during the core-flooding experiments.

Recipe	Projections Counts	Exposure time(s)	Camera binning	Resolution(μm)	Image size (pixel)	Objective
High-resolution scan	3201	6.5	1	2.5	2032 × 2032	4.0 ×
Low-resolution scan	1601	2.0	2	5	1014 × 1014	4.0 ×

The scan recipes as listed in Table 3 were prepared to study the pore-scale displacement physics in three different locations of the sample (i.e., A, B, and C) as demonstrated in the dotted square regions in Figure 3. These locations were selected to allow the study of pore fluid occupancies and fluid movements at different morphological sites of the sample. This allowed the construction of fluid saturation profiles at these locations, which, in turn, helped to develop insight into the most favorable flow pathways along the core sample.

Data acquisition and processing

Avizo™ 9.0.1 and PerGeos™ 1.0.1 software were utilized to visualize the reconstructed tomograms obtained from the micro-CT scanner. ImageJ software was also used to visualize the images from the medical CT scanner. The micro-CT tomograms were processed prior to the final visualizations by the following steps: (1) Applying secondary referencing method for some of the images with ring artifact, (2) filtering the images using mainly the non-local means filter and other types of filter modules toremove noise and any artifacts, such as salt and pepper that might not have been eliminated during the reconstruction process (3) using different arithmetic operations toget the three-phase pore map by multiplying the reference scan by the flooded scan, (4) segmentation and thresholding, and (5) quantitative analysis to calculate saturation, and porosity.More details about these steps can be found elsewhere (Alizadeh *et al*. 2014).

Results and discussion

In this section, the results of the pore-scale experimental study on the matrix-fracture interactions in the presence of spreading oil layers are presented. The pore fluid occupancies under three-phase flow were visualized employing an X-ray microtomography technique with a resolution of 2.5 microns. In the following sections, the results of the two-phase flow condition (*i.e.*, drainage by oil injection followed by

waterflood) are first discussed. Then, the relevant pore-scale observations under tertiary gas injection on the impact of the spreading phenomenaon oil recovery are covered.

Primary Drainage by Oil

After establishing a fully brine saturated core sample, oil was injected at an initial flow rate of 0.0001 ml/min followed by an incremental increase to 0.004 ml/min. This resulted in an average initial water saturation (S_{wi}) of 24%. During the ramping process of the oil flow rate, oil, as the non-wetting phase with respect to brine, started initially to fill the fracture pathway. Then, oil gradually invaded more brine-filled pores in the matrix as the capillary pressure increased. Since the medium was water-wet, brine formed thin wetting films on the roughness of the fracture walls and resided as layers in the corners of the pores whereas oil occupied the centers as shown in Figure 5 (a). The brine continuity was maintained through these wetting films with a non-negligible hydraulic conductivity.

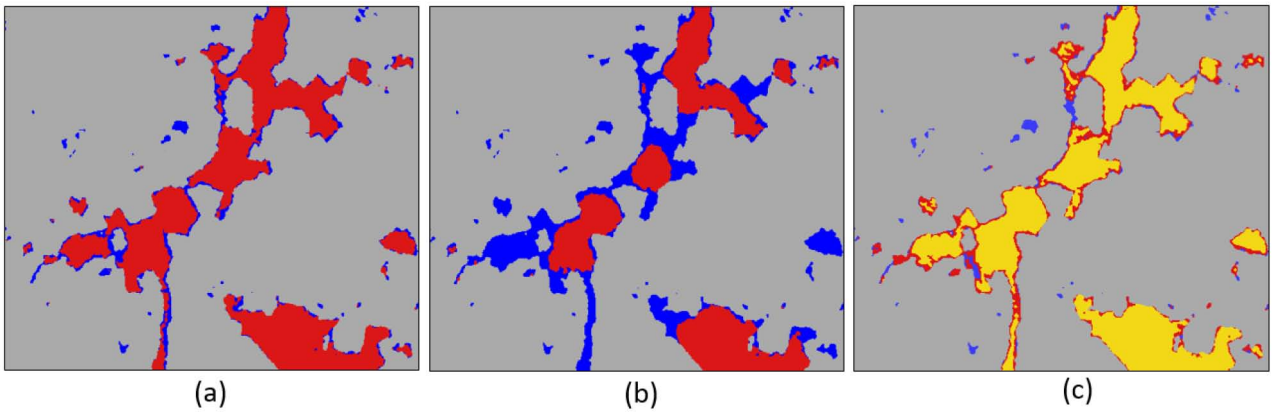

Figure 5—Two-dimensional cross-sectional views of a pore that is connected to the fracture at Location A after (a)primary drainage, (b) brine imbibition and (c)tertiary gas injection (resolution 2.5 μm). Blue, red, yellow, and gray colors represent brine, oil, gas, and grains, respectively.

Waterflooding

After reaching an initial average water saturation of 24%, brine was injected into the core at an initial flow rate of 0.0001 ml/min followed by a gradual increase to 0.004 ml/min. These flow rates were determined to be within the capillary-dominated flow regime (Ca ~1×10^{6}). Water, as the wetting-phase, started to imbibe into small matrix pore elements and narrow fracture aperture. Brine layers were observed to be resided in the corners of the pore elements. As the brine flow rate was increased, local oil-water capillary pressure reduced and in turn, water invaded the larger pores and thicker fracture openings based on the imbibition threshold capillary pressure. At the highest brine flow rate (*i.e.*, 0.004 ml/min), the swelling of the brine layers increased which forced the oil to be, in turn, trapped in large pores and thicker fracture openings through the snap-off displacement mechanism as seen in Figure 5 (b). This displacement phenomenon can be seen in a three-dimensional view of a single fracture opening in Figures 6 (b) before waterflood and 6 (c) after waterflood where the non-wetting phase was trapped in the center of that fracture opening. The brine phase in this figure was digitally eliminated to showa single fracture opening occupancy of an isolated oil globule. Trapping of the oil phase can also be seen in figure 7 (a) where oil was trapped in thicker fracture openings and larger pores.

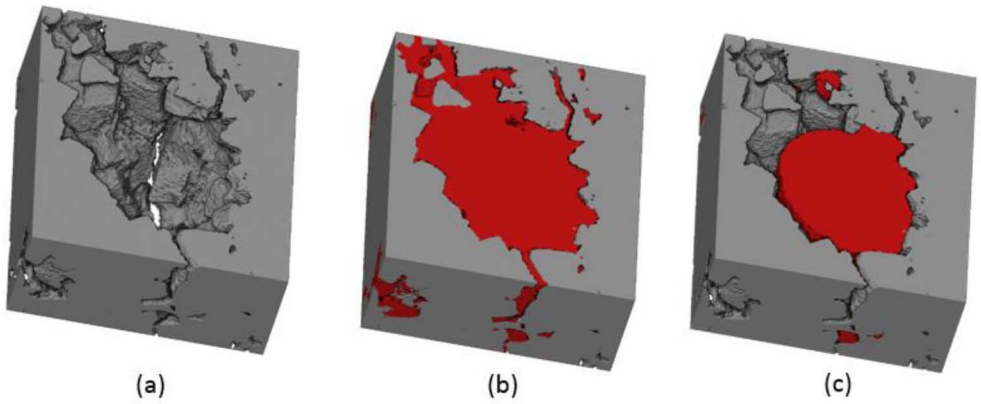

Figure 6—Three-dimensional views of a fracture opening at Location A showing an oil globule trapped during waterflood (resolution 2.5 μm). Red and gray colors represent oil, and grains, respectively.

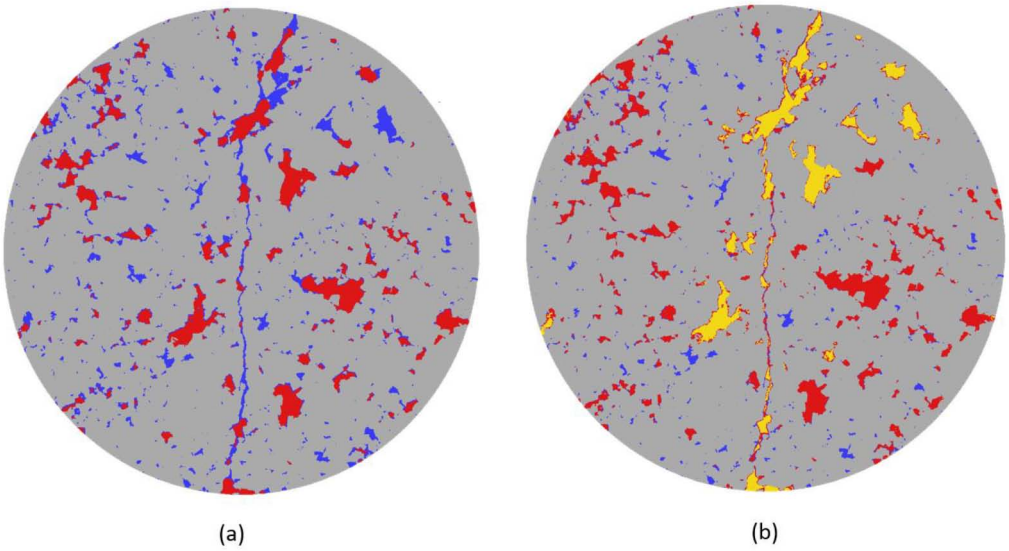

Figure 7—Two-dimensional cross-sectional views of the fracture at Location A after (a) brine imbibition (waterflooding) and (b) tertiary gas injection (resolution 2.5 μm). Blue, red, yellow, and gray colors represent brine, oil, gas, and grains, respectively.

Tertiary Gas Injection

After the completion of waterflooding to residual oil saturation (S_{or} of 52%), the most non-wetting phase (*i.e.*, nitrogen gas) was introduced into the core at an initial flow rate of 0.001 ml/min. The injected gas primarily propagated into the fracture conduit as it was the least resistant path due to the negligible gas-brine threshold capillary pressure as seen in Figures 7 (b) and 8. At this low flowrate of gas, there was no observation of a significant sweep efficiency of oil from the pores in the matrix adjoining the fracture. When the gas phase entirely filled the fracture, the gas pressure was adequate to overcome the matrix capillary pressure. Since the wetting phase (*i.e.*, brine) was mobile and the intermediate wetting phase (*i.e.*, oil) in the neighboring matrix was trapped, gas, as the most non-wetting phase, displaced the brine first and then reached the trapped oil globules. After reaching these globules, gas started to displace oil. As the gas flow rate increased resulting in increasing the gas-water capillary pressure, oil started to evolve and form spreading layers between brine and gas as seen in Figure 5 (c). At this gas pressure, the oil globules were reconnected, and oil was displaced through continuous and stable spreading oil layers. Gas started to displace oil which, in turn, displaced brine. As illustrated in the ternary diagram in Figure 9,the gas displaced a significant amount of brine at a relatively low flow rate of gas and then more oil. As shown in the diagram, the saturation of oil at the end of gas injection reached as low as 14%. Also, it was observedthat

in the fracture location of the sample, the average gas saturation profile in the direction perpendicular to thedirection of the gas flow was not uniform as seen in Figure 7 (b). The pores on theright side of the fracture were relatively invaded more than the left side. The oil phase in the larger pores surrounding the fracture was invaded earlier than those that were far away from the fracture. Thiswas expected to be a consequence the gas phase accessibility to the network of pores that were directly connected to the fracture. Less threshold pressurewas required for the gas in the fracture to invade the closer pore elements than finding a pathway of pores and throats through the matrix to invade elements away from the fracture with higher threshold capillary pressures as illustrated in Figure 7 (b) and 8.

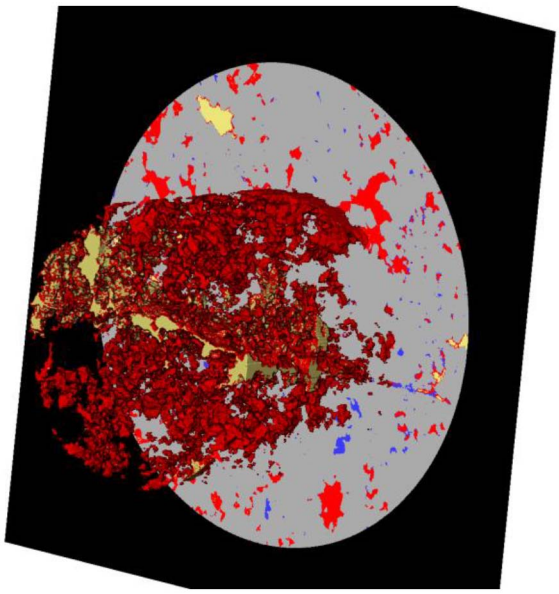

Figure 8—Three-dimensional view of a three-phase segmented image at Location A showing the gas invasion into the fracture at low gas flow rate (resolution 2.5 μm). Blue, red, yellow, and gray colors represent brine, oil, gas, and grains, respectively.

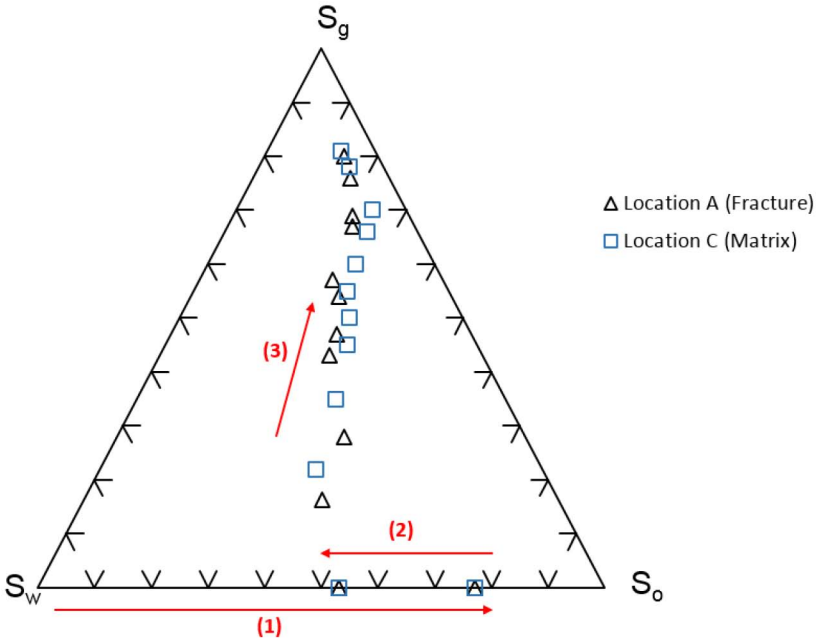

Figure 9—Three-phase saturation trajectory. The core sample initially saturated with 100% water was subjected to (1) primary oil drainage to initial water saturation, (2) followed by a waterflooding to residual oil saturation, and then (3) gas injection.

The observed spreading layers in the micro-CT images were expected to have a significant role in maintaining the connectivity of oil from the matrix to oil in the fracture. These observations were consistent with some micromodel and other experimental studies presented in the literature under which some thinner oil layers were observed at a certain range of capillary pressures (Keller *et al*. 1996; Khalaydjian *et al.*1995; Vizika *et al*. 1996). As depicted in Figure 10 when gas invaded more fracture-adjacent pores as the gas flow rate increased, the hydraulic conductivity of the oil phase (the faded red color phase in the figure) was connected from an adjacent pore element in the matrix to the fracture conduit. The Euler characteristics were used to quantify the oil connectivity from the micro-CT images. The method has frequently been used in literature to quantify the connectivity of elements in a network (Jacobs*et al*. 2000; Feali*et al*. 2012). The negative and positive Euler characteristic numbersrepresent highly connected and isolated elements, respectively (Feali *et al*. 2012). The computed Euler characteristic value for the oil phase in this study was negative, which confirms the connectivity of the oil phase.

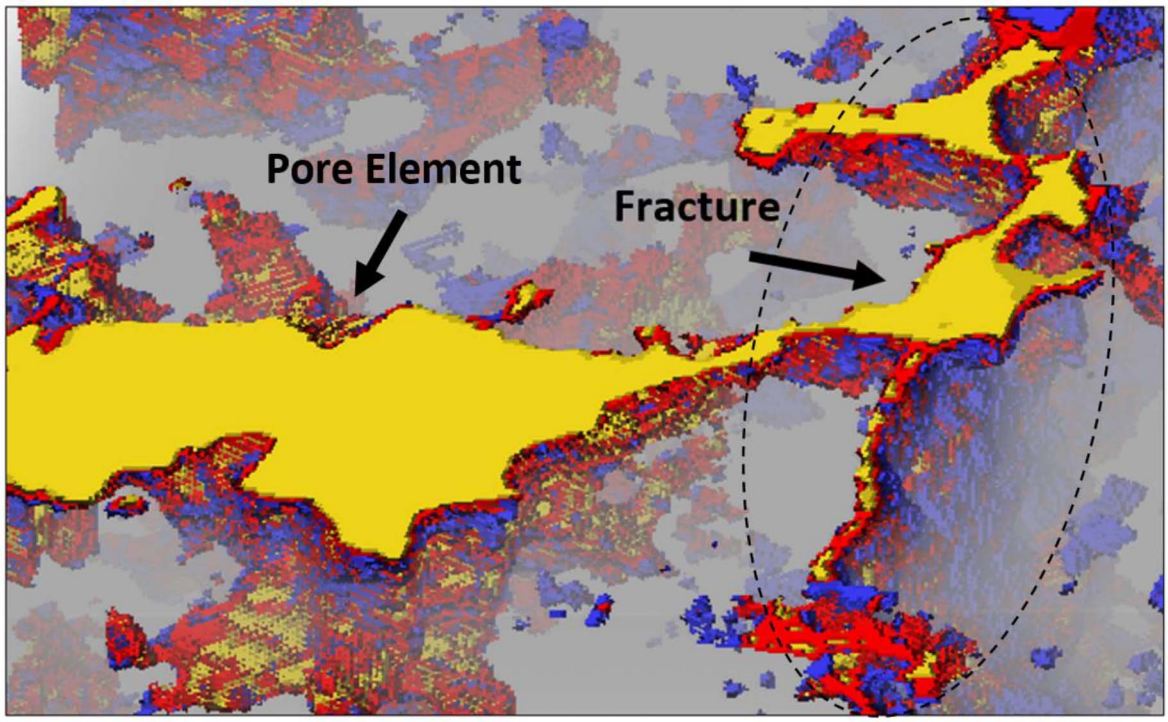

Figure 10—Three-dimensional viewof a three-phase segmented images at Location A showing the connectivity of the oil phase (faded red color) from a pore element adjacent to the fracture (resolution 2.5 µm). Faded blue, red, yellow, and gray colors represent brine, oil, gas, and grains, respectively.

Concluding remarks

Based on the micro-scale experimental study performed, it was concluded that:

- Direct visualization of the micro-CT images confirmed the substantial role of the spreading layers in maintaining the hydraulic conductivity and the phase connectivity of the reconnected trapped oil blobs from the matrix to the fracture.
- Comparison of the pore and fracture fluid configurations using the micro-CT images clearly demonstrated the importance of the matrix-fracture interaction during gas injection and helped to probe the dominant displacement mechanisms under three-phase flow.
- Negative Euler characteristics number computed for the oil phase confirmed its connectivity throughout the pore space based on the spreadability of the system.

- The saturation profile over the course of the gas injection showed that brine was predominately produced first since it was well-connected. Oil was then displaced through the spreading layers.
- The displacement of oil, especially at higher flow rates,was mainly governed by the stability and the hydraulic connectivity of the spreading oil layers that maintained the continuity of the oil phase from the matrix to the fracture.

Acknowledgements

The author would like to acknowledge the financial support of Saudi Aramco, Hess Corporation, Kuwait Oil Company, and the School of Energy Resources (SER) at the University of Wyoming. The experimental support from Dr. Amir Hossein Alizadeh and Evan W. Lowry is appreciated. The author isimmensely grateful to Prof. Mohammad Piri for the technical support and guidance as well as for granting access to the High Bay Research Facility - Center of Innovation for Flow through Porous Media (COIFPM) at the University of Wyoming.

References

Adamson A.W. and Gast A.P., 1967. *Physical chemistry of surfaces*.

Alajmi A.F. and Grader A.S., 2000. Analysis of fracture-matrix fluid flow interactions using X-ray CT. In *SPE Eastern Regional Meeting*. Society of Petroleum Engineers.

Alajmi A.F., 2003. *The influence of a fracture tip on two-phase flow displacement processes* (Doctoral dissertation, The Pennsylvania State University).

Alizadeh A.H. and Piri M. 2014. The Effect of saturation history on three-phase relative permeability: An experimental study. *Water Resources. Res*., **50**, 1636-1664. doi:10.1002/2013WR014914.

Alizadeh A.H., Khishvand M., Ioannidis M.A. et al. 2014. Multi-scale experimental study of carbonated water injection: An effective process for mobilization and recovery of trapped oil. *Fuel* **132**, 219-235.

Alvarado F.E., Grader A.S., Karacan O. and Halleck P.M., 2004. Visualization of three phases in porous media using micro computed tomography. *Petrophysics*, **45**(06).

Andrä H., Combaret N., Dvorkin J., Glatt E., Han J., Kabel M., Keehm Y., Krzikalla F., Lee M., Madonna C. and Marsh M., 2013. Digital rock physics benchmarks—Part I: Imaging and segmentation. *Computers & Geosciences*, **50**, pp. 25-32.

Blunt M., Zhou D. and Fenwick D., 1995. Three-phase flow and gravity drainage in porous media. In *Multiphase Flow in Porous Media* (pp. 77-103). Springer Netherlands.

Blunt M.J., 2017. *Multiphase flow in permeable media: a pore-scale perspective*. Cambridge University Press.

Chatzis I., Kantzas A. and Dullien F.A.L., 1988. On the investigation of gravity-assisted inert gas injection using micromodels, long Berea sandstone cores, and computer-assisted tomography. In SPE Annual Technical Conference and Exhibition. Society of Petroleum Engineers.

Dumore J.M. and Schols R.S., 1974. Drainage capillary-pressure functions and the influence of connate water. *Society of Petroleum Engineers Journal*, **14**(05), pp.437-444.

Feali M., Pinczewski W., Cinar Y., Arns C.H., Arns J.Y., Francois N., Turner M.L., Senden T. and Knackstedt M.A., 2012. Qualitative and quantitative analyses of the three-phase distribution of oil, water, and gas in bentheimer sandstone by use of micro-CT imaging. *SPE Reservoir Evaluation & Engineering*, **15**(06), pp.706-711.

Guo H., Aziz N.I. and Schmidt L.C., 1993. Rock fracture-toughness determination by the Brazilian test. *Engineering Geology*, **33**(3), pp.177-188.

Haugen Å., Fernø M.A., Bull Ø. and Graue A., 2010. Wettability impacts on oil displacement in large fractured carbonate blocks. *Energy & Fuels*, **24**(5), pp.3020-3027.

Hirasaki G.J., 1993. Structural interactions in the wetting and spreading of van der Waals fluids. *Journal of adhesion science and technology*, **7**(3), pp.285-322.

Islam M.R., 2014. *Unconventional Gas Reservoirs: Evaluation, Appraisal, and Development*. Elsevier.

Jacobs K., Seemann R. and Mecke K., 2000. Dynamics ofStructure Formation in Thin Liquid Films: A Special Spatial Analysis. In *Statistical Physics and Spatial Statistics*, pp. 72-91. Springer Berlin Heidelberg.

Kalaydjian F., Vizika O., Moulu J.C. and Munkerud P.K., 1995. The role of wettability and spreading in gas injection processes under secondary conditions. *Geological Society*, London, Special Publications, **84**(1), pp.63-71.

Keller A.A., Blunt M.J. and Roberts A.P.V., 1997. Micromodel observation of the role of oil layers in three-phase flow. *Transport in Porous Media*, **26**(3), pp.277-297.

Lu J., Goudarzi A., Chen P., Kim D.H., Britton C., Delshad M., Mohanty K.K., Weerasooriya U.P. and Pope G.A., 2012. Surfactant enhanced oil recovery from naturally fractured reservoirs. In SPE Annual Technical Conference and Exhibition. Society of Petroleum Engineers.

Manrique E.J., Muci V.E. and Gurfinkel M.E., 2007. EOR field experiences in carbonate reservoirs in the United States. *SPE Reservoir Evaluation & Engineering*, **10**(06), pp.667-686.

Øren P.E. and Pinczewski W.V., 1994. The effect of wettability and spreading coefficients on the recovery of waterflood residual oil by miscible gasflooding. *SPE Formation Evaluation*, **9**(02), pp.149-156.

Øren P.E. and Pinczewski W.V., 1995. Fluid distribution and pore-scale displacement mechanisms in drainage dominated three-phase flow. In *Multiphase Flow in Porous Media* (pp. 105-133). Springer Netherlands.

Piri M. and Blunt M.J., 2004. Three-phase threshold capillary pressures in noncircular capillary tubes with different wettabilities including contact angle hysteresis. *Physical review E*, **70**(6), p.061603.

Piri M., Recirculating. Constant back pressure core-flooding apparatus and method., *Patent W02012/082797* (University of Wyoming, 2012).

Rowlinson J.S. and Widom B., 2013. *Molecular theory of capillarity*. Courier Corporation.

Sabti M., Alizadeh A.H. and Piri M., 2016a. Three-Phase Flow in Fractured Porous Media: Experimental Investigation of Matrix-Fracture Interactions. In SPE Annual Technical Conference and Exhibition. Society of Petroleum Engineers (Dubai, UAE).

Sabti M., Alizadeh A.H. and Piri M., 2016b. *Matrix-fracture interation during gas injection: A pore-scale experimental study, SCA2016-029*

Vizika O., 1993. *Effect of the spreading coefficient on the efficiency of oil recovery with gravity drainage*. American Chemical Society, Washington, DC (United States).

Wildenschild D. and Sheppard A.P., 2013. X-ray imaging and analysis techniques for quantifying pore-scale structure and processes in subsurface porous medium systems. *Advances in Water Resources*, **51**, pp.217-246.

Zhou D. and Blunt M., 1997. Effect of spreading coefficient on the distribution of light non-aqueous phase liquid in the subsurface. *Journal of Contaminant Hydrology*, **25**(1-2), pp.1-19.